https://doi.org/10.5194/egusphere-2026-6637
Preprint. Discussion started: 16 November 2026
© Author(s) 2026. CC BY 4.0 License.

Partitioning Local and Long-Range Refractory Black Carbon in the High Arctic: Microphysical Aerosol Properties from the SP2-XR in Northwestern Greenland

Alia L. Khan[1,2], Darrel G. Baumgardner[3], Peng Xian[4], Ella Hall[1,2], Filippo Cali Quaglia[5], Giovanni Muscari[5]

[1]Department of Aerospace Engineering Sciences, University of Colorado – Boulder, Department of Environmental Sciences, Boulder, CO, USA;
[2]Western Washington University, Bellingham, WA, USA;
[3] Droplet Measurement Technologies, Inc., Boulder, CO, USA;
[4]Aerosol and Radiation Section of the Marine Meteorology Division, Naval Research Laboratory, Monterey, California, USA,
[5]Istituto Nazionale di Geofisica e Vulcanologia, Rome, Italy

Correspondence to: Alia Khan, alia.khan@colorado.edu

Abstract

Black carbon deposition on the Greenland Ice Sheet significantly reduces surface albedo and accelerates melt, yet the microphysical properties that distinguish local emissions from long-range wildfire smoke remain poorly constrained. We characterized single-particle refractory black carbon (rBC) using an Extended Range Single Particle Soot Photometer (SP2-XR) at the Thule High Arctic Atmospheric Observatory in northwest Greenland from June to September 2024. By pairing real-time measurements with local meteorology and Navy Aerosol Analysis and Prediction System Reanalysis (NAAPS-RA) smoke concentrations, we partitioned aerosol measurements into local, long-range, and mixed regimes. Here we report microphysical properties of rBC as core mass-equivalent diameter (EMD), equivalent optical diameter (EOD), and equivalent coating thickness (ECT). Fresh emissions from local infrastructure (Pituffik Space Base) were characterized by larger median rBC mass cores (EMD = 196.3 nm), smaller total optical diameters (EOD = 316.1 nm), and thin coatings (ECT = 56.7 nm). In contrast, long-range biomass burning smoke from North America exhibited smaller rBC cores (EMD = 184.7 nm), significantly larger overall optical diameters (EOD = 343.1 nm; $p < 0.01$) and statistically significantly thicker secondary aerosol coatings (ECT = 60.8 nm; $p < 0.05$). Consistent with previous studies, this inverse relationship between core and optical size provides near-surface validation that secondary non-rBC coating accumulation drives the total optical volume of aged Arctic smoke. As Arctic shipping, local industrialization, and high-latitude wildfires increase, these distinct optical and microphysical signatures provide essential observational constraints for climate models to accurately simulate BC optical properties, atmospheric deposition, and snow-albedo feedbacks.

https://doi.org/10.5194/egusphere-2026-6637
Preprint. Discussion started: 16 November 2026
© Author(s) 2026. CC BY 4.0 License.

1. Introduction:

Black carbon (BC) is a potent, short-lived climate forcer that plays an outsized role in Arctic climate dynamics. In the Arctic environment, BC exerts a dual warming effect: it absorbs incoming solar radiation in the atmosphere, and critically, it reduces surface albedo when deposited onto snow and ice (Bond et al., 2013). This deposition-induced albedo reduction is particularly concerning for the Greenland Ice Sheet (GrIS), where dark particulates increase the absorption of shortwave radiation, triggering positive feedback loops that accelerate surface melting and contribute to global sea-level rise (Flanner et al., 2007). Furthermore, the seasonal patterns of Arctic aerosols (Schmale et al., 2022) may be shifting (Xian et al., 2022a), responding to, and helping to drive, changes to the Arctic climate (Schmale et al., 2021). To accurately predict future melt scenarios, regional climate models require accurate constraints on both the concentration and microphysical properties of BC depositing in the high Arctic.

Emissions from North America and Eurasia are frequently transported into the high northern latitudes, manifesting historically as winter and spring "Arctic Haze," (Frossard et al., 2011; Schmale et al., 2022) and increasingly as summer intrusions of biomass burning smoke (Law and Stohl, 2007; Stohl et al., 2013). Indeed, boreal wildfires have become a dominant source of long-range transported Arctic BC during the melt season (Khan et al., 2023; Xian et al., 2022a). However, as the Arctic warms and sea ice retreats, the region is experiencing a steady increase in local industrialization and accessibility. Local anthropogenic emissions stemming from shipping (Heutte et al., 2026), coal mining (Khan et al., 2017b) and military or research infrastructure as demonstrated in the Antarctic (Cordero et al., 2022), are emerging as highly concentrated, continuous point sources of BC (Khan et al., 2017a) that threaten local snow and ice surfaces (Eckhardt et al., 2015; Winiger et al., 2017). Although bulk BC mass transport to the Arctic is well-documented, characterizations of single-particle mixing states and coating characteristics over Greenland remain sparse, leaving significant uncertainties in how these aged plumes evolve during long-range transport (Adachi et al., 2026).

https://doi.org/10.5194/egusphere-2026-6637
Preprint. Discussion started: 16 November 2026
© Author(s) 2026. CC BY 4.0 License.

Understanding the relative climate impact of these two distinct regimes requires examining the microphysical evolution of the particles themselves. As BC travels thousands of kilometers from mid-latitude wildfires (Doherty et al., 2010), it undergoes significant atmospheric aging. While total particle concentrations decrease due to atmospheric dilution and wet scavenging, the surviving particles acquire thick coatings of secondary organic aerosols and sulfates, significantly altering their hygroscopicity and deposition velocity (Kodros et al., 2018; Zanatta et al., 2018). In contrast, fresh local emissions have not undergone this extensive aging process. As a result, they are characterized by smaller total particle diameters and thinner individual coatings before atmospheric condensation builds up a thick, secondary shell around the rBC core (Wang et al., 2011). While these physical differences are well documented in laboratory settings and lower latitudes, ground-level, high-resolution partitioning of aged versus fresh BC microphysics in the high Arctic, especially near the GrIS, remains sparse.

To better constrain the impacts of BC deposition on GrIS melt, it is essential to differentiate local contamination from long-range transport in observational datasets. In this study, we present high-resolution measurements of aerosol particles, with and without refractory black carbon (rBC), measured with an Extended Range Single Particle Soot Photometer (SP2-XR) at the Thule High Arctic Atmospheric Observatory (THAAO) in northwest Greenland. By pairing direct microphysical measurements with the Navy Aerosol Analysis and Prediction System Reanalysis (NAAPS-RA) model of wildfire smoke flux data and local meteorology, we categorize aerosol transport into local, long-range, and mixed regimes. Ultimately, this work aims to characterize the distinct microphysical signatures, specifically size and coating distributions, of nearby fossil-fuel emissions from the Pituffik Space Base compared to transported North American wildfire smoke, providing necessary observational constraints for future Arctic climate modeling.

2. Methods

2.1. Study Area and Site Description

An SP2-XR was installed at the THAAO (76.5°N, 68.8°W, 220 m asl, www.thuleatmos-it.it), located on a hill south of the Pituffik Space Base, about 3 km inland from the coast of Greenland and about 20km west of the Greenland Ice Sheet on ice-free land (GrIS; Fig. 1a) to complement airborne measurements by the NASA ARCSIX field campaign (Taylor et al., 2026).

https://doi.org/10.5194/egusphere-2026-6637
Preprint. Discussion started: 16 November 2026
© Author(s) 2026. CC BY 4.0 License.

The Pituffik Space Base has an airstrip, with regular, daily aircraft traffic, northeast of where the SP2-XR was installed, and a powerplant located north of the SP2-XR location, which are both potential local sources of rBC. The study site is also located east of North America, which is a major source region for biomass burning smoke from wildfires transported to Greenland.

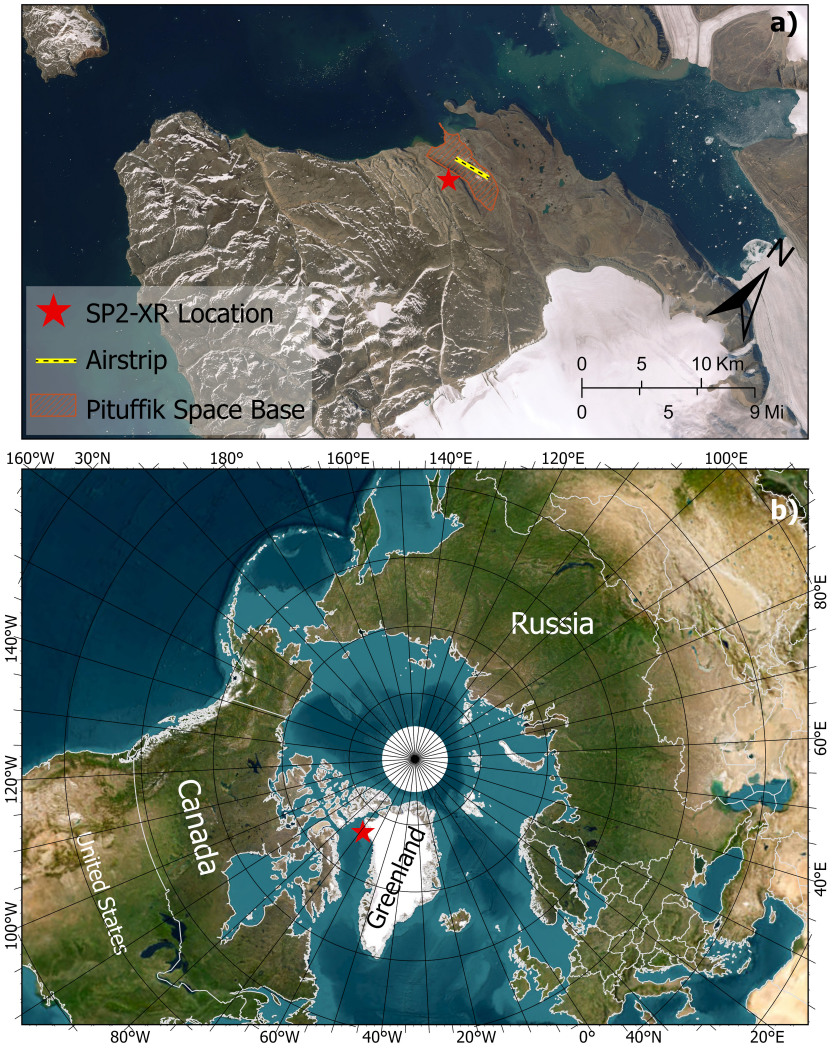


Fig 1. a) Location of the SP2-XR (star symbol) relative to the Pituffik Space Base and the airstrip; **b)** Location of the SP2-XR in relation to North America and the greater Arctic. The base map source was designed and developed by ESRI and accessed via ArcGIS Pro World Imagery | Powered by Esri.

https://doi.org/10.5194/egusphere-2026-6637
Preprint. Discussion started: 16 November 2026
© Author(s) 2026. CC BY 4.0 License.

The SP2-XR made continuous measurements for 102 days from 06/19/2024 – 09/29/2024. It was installed on a shelf inside the THAAO building, and the 1.3 cm diameter intake tube was routed through a small hole in the wall and secured to a roof-mounted support (Figure 2a). The electrically grounded, 1.3 cm diameter intake tube was oriented vertically but bent slightly to prevent precipitation from entering the tube (Figure 2b). Inertial particle losses in the bends and losses by diffusion to the walls were estimated using the spreadsheet, aerocalc.xls, widely used by aerosol scientists, and taking into account the 1.0 cm^3 s^{-1} flowrate. For particles in the size range of the SP2-XR, particle losses were less than 0.01%.



Fig 2. a) SP2-XR setup inside THAAO building on a shelf to decrease the distance the intake tube had to travel to reach the top of the roof outside the building; **b)** SP2-XR intake tube routed through a small hole in the side of the building and secured to a mount with a slight bend in the tubing.

2.2. Navy Aerosol Analysis and Prediction System - Reanalysis (NAAPS-RA) Smoke Flux Data

The NAAPS-RA is a global aerosol reanalysis model that provides 6-hourly, 3-dimensional tropospheric concentrations and optical properties of major aerosol species

https://doi.org/10.5194/egusphere-2026-6637
Preprint. Discussion started: 16 November 2026
© Author(s) 2026. CC BY 4.0 License.

including dust, anthropogenic and biogenic fine aerosols (ABF), sea salt, and biomass burning smoke at a 1º x 1º latitude, longitude resolution, for 25 vertical levels, from 2003 to the present (Lynch et al., 2016; Xian et al., 2022b). Smoke particles from biomass burning are derived from near-real time satellite-based thermal anomaly data that are used to construct smoke source functions (Reid et al., 2009), with additional orbital corrections and regional tunings (Lynch et al., 2016). The NAAPS-RA has been shown to have great skill in capturing transported smoke from the mid-latitude region to the Arctic (Khan et al., 2017a; Markowicz et al., 2016; Ranjbar et al., 2019; Xian et al., 2022b). In this study, we use the daily surface concentration of biomass burning smoke, which is a daily-average value given in μg m^{-3}, to compare to measurements collected by the SP2-XR and help distinguish between sources of rBC.

2.3. THAAO Meteorological Data

Wind speed (m/s) and wind direction (º) measurements were collected every minute at the THAAO meteorological towers located about 30 m from the building at a height of 5 m agl (Ciardini et al., 2026). Wind direction data was used to classify potential local sources of aerosol transport to the SP2-XR location.

2.4. Measurement methodology

The SP2-XR is a version of the SP2-D, which uses laser induced incandescence (LII) to derive rBC (Schwarz et al., 2006; Stephens et al., 2003). Through calibration the mass of rBC in individual particles is extracted from the incandescence signal. Although some pure metals will also incandesce, as discussed by Schwarz et al. (2006), the majority will be rBC. In addition to measuring rBC with LII, the instrument also measures the light that scatters from each particle in the range of equivalent optical diameters (EOD) from 100-500 nm, regardless of whether they incandesced, i.e. contained rBC. From here forward, incandescing particles will be referred to as rBC and the particles that scatter light will be designated as scattering particles. There are some particles whose EOD is below the detection threshold of scattered light but that have rBC whose incandescence can be detected and quantified.

One of the principal metrics that will be used in this study to correlate with the age and origins of the rBC is the mixing state, a parameter that describes the amount of non-incandescing material that is mixed with the rBC. The mixing state has been defined in a number of ways by those who make measurements with the SP2. The definition that will be used here is that of

https://doi.org/10.5194/egusphere-2026-6637
Preprint. Discussion started: 16 November 2026
© Author(s) 2026. CC BY 4.0 License.

coating thickness (Schwarz et al., 2008a, b) which compares the EOD of the particle to its equivalent mass diameter (EMD). The EMD is defined as that diameter of rBC if it is collapsed into a sphere with a density of 1.6 g cm^{-3} . Although the difference between the EOD and EMD has been referred to in previous studies as the coating thickness, from here forward we will use the terminology Equivalent Coating Thickness (ECT) to highlight that this is not an actual geometric thickness but is rather a surrogate of the mixing state. Given the errors in EOD of ±30%, due to uncertainties in refractive index, shape and partial evaporation, and error in EMD of approximately ±50%, due to uncertainties in densities and fractal shape, the propagated error in ECT is approximately ±60%. Although the reader will be reminded of this uncertainty throughout the remainder of this manuscript, we are more interested in relative changes in the ECT rather than absolute values.

Descriptions and units of each of the variables directly measured from the SP2-XR can be found in Table S1 and the derived variables in Table S2.

2.5. Local Contamination vs. Long-Range Transport Events

In order to compare with the NAAPS-RA model, the SP2-XR measurements were also averaged to provide a daily value for each variable, matching the temporal structure of the NAAPS-RA biomass burning smoke surface concentration data. To isolate when the surface smoke concentration was especially high, days when the concentration was above the median value (0.115 µg m^{-3}) were classified as high smoke days. To identify potential long-range smoke transport, the days with high smoke concentration were filtered to only include days when the average wind direction was coming from the West, South, Southwest, or Southeast, which could indicate smoke transport from Canada or from shipping ports in Southern Greenland. Local infrastructure plume passages were identified on days dominated by wind directions from local source sectors (Pituffik Space Base, power plant, airstrip: N, NE, E) during low regional smoke conditions (NAAPS-RA $< 0.115\ \mu g\ m^{-3}$). To ensure that analyzed local intervals reflected active operational emissions rather than clean background air, an operational plume-screening threshold (rBC concentration > 3.18 particles cm^{-3}) was applied. Because concentration parameters served as part of the initial spatial/operational filter, our scientific evaluation focuses independently on single-particle microphysical properties (ECT, EOD, and EMD) that were not used in regime classification. A “mixed” case was classified as when the surface smoke

https://doi.org/10.5194/egusphere-2026-6637
Preprint. Discussion started: 16 November 2026
© Author(s) 2026. CC BY 4.0 License.

concentration was above the median value, but the wind was coming from the North, Northwest or Northeast, indicating potential transport of aerosols from the power plant north of the measurement site.

2.6. Statistical Analysis

NAAPS Model and SP2-XR Comparison

The daily smoke, dust and ABF data were not normally distributed, therefore, the median was used to identify high deposition days where smoke, dust, or ABF surface concentrations were above the median value, while those below the median value were considered "low" deposition days. The median smoke concentration was 0.115 μg m^{-3} day^{-1}, the median dust concentration was 0.47 μg m^{-2} day^{-1}, and the median ABF concentration was 0.18 μg m^{-3} day^{-1} (Figure 3). Non-parametric Wilcoxon Rank-Sum tests (W test statistic) were used to compare particle attributes measured by the SP2-XR between high and low smoke, dust and ABF events. Chi-squared test statistics analyses (χ^2(degrees of freedom)) are applied to explore statistically significantly differences between local, long-range, and mixed transport events described in the next section.

Local / Long-Range / Mixed Transport Comparison

Assumptions of normality and homogeneity of variance were assessed using residual Q–Q plots and Levene's tests. One of the five variables measured by the SP2-XR (scattering particle concentration) during local, long-range and mixed transport events violated the assumptions required for analysis of variance (ANOVA) testing. Therefore, Kruskal–Wallis tests were applied to all variables as a non-parametric alternative to assess differences in particle attributes among transport types. When there were significant differences among transport types, Dunn's post-hoc test with Benjamini-Hochberg correction was used to determine which groups specifically differ.

3. Results/ Discussion

To preface the following discussion, a brief overview of how rBC properties relate to source and age is useful to describe how and why we relate the Greenland SP2-XR measurements to the air mass origins and history. Incomplete combustion is the source of most

https://doi.org/10.5194/egusphere-2026-6637
Preprint. Discussion started: 16 November 2026
© Author(s) 2026. CC BY 4.0 License.

rBC, which also depends on the fuel that is burning and its temperature (Bond et al., 2013). High temperature combustion, e.g. from jet engines and power plants, produce high concentrations of very small rBC that will very rapidly coagulate into larger particles, whereas biomass burning such as from wildfires produce much larger rBC in lower numbers. Likewise, there are many gases that form in high temperature combustion that will subsequently condense on rBC surfaces that contribute to the ECT derived with the SP2-XR. Similar condensation on rBC will happen in air masses leaving wildfires, but the gases will be in lower concentration and hence the condensation process takes longer. This complexity of rBC interactions with gases, as well as with other aerosols, is what makes interpretation of the SP2-XR measurements challenging.

To contextualize the atmospheric conditions over the THAAO during the summer of 2024, we first evaluated the regional aerosol surface concentration using the NAAPS-RA modeled daily surface concentrations. Across the entire sampling window (102 days from June 19 to September 29, Figure 3), dust was the dominant aerosol species by mass, exhibiting the highest overall seasonal median surface concentration, followed by ABF, and biomass burning smoke (Table 1). The same trend was observed for cumulative monthly total surface concentration. While dust maintained the highest median concentration and total surface concentration across the summer season, the three aerosol species exhibited distinct monthly variations that reflect changing seasonal transport pathways and source strengths.

Biomass burning smoke produced from wildfires peaked sharply in August, with a doubling of the monthly median. The total monthly surface concentration in August was also more than half the total summer season concentration. This late-summer surge is consistent with peak wildfire activity in North America (Buchholz et al., 2022). The August smoke maximum also exceeds the dust maximum.

Both dust and ABF concentrations increased over the summer, culminating with their highest median concentrations in September. The elevated late-season dust concentrations may point to enhanced regional bare ground exposure as shown by enhancement of some metals naturally occurring in the nearby soil (Becagli et al., 2020) due to progressive seasonal snow melt, as well as high-latitude permafrost thaw. The elevated ABF does not follow previous reports of a maximum in Spring due to Arctic Haze (Frossard et al., 2011), potentially suggesting a rise due to increased regional anthropogenic activities such as enhanced shipping (Heutte et al., 2026) due to waning Arctic sea ice (Zhao et al., 2025). However, this could also be due to the

https://doi.org/10.5194/egusphere-2026-6637
Preprint. Discussion started: 16 November 2026
© Author(s) 2026. CC BY 4.0 License.

241 complexity of Arctic aerosol-climate interactions, the evolution and transport of Arctic aerosols,
242 and their effects on cloud microphysics (Schmale et al., 2021).
243
244 **Table 1:** Seasonal NAAPS-RA daily and cumulative monthly surface concentration summary
245 table (μg m^{-3}). Median (M) values were used to separate the high and low bins for Table 2.

	July		**August**		**Sept**		**Total Season (6/19/24 - 9/29/24)**	
	M (Q1-Q3)	**Max**	**M (Q1-Q3)**	**Max**	**M (Q1-Q3)**	**Max**	**M (Q1-Q3)**	**Max**
Smoke	0.07 (0.04 - 0.12)	0.38	0.21 (0.13 - 0.44)	1.95	0.12 (0.08 - 0.23)	0.39	0.11 (0.06 - 0.23)	1.95
Dust	0.35 (0.27 - 0.51)	0.96	0.52 (0.36 - 0.8)	1.78	0.73 (0.43 - 1.33)	3.36	0.47 (0.3 - 0.73)	3.65
ABF	0.13 (0.09 - 0.17)	0.27	0.17 (0.12 - 0.21)	0.68	0.43 (0.3 - 0.61)	1.53	0.18 (0.12 - 0.28)	1.53
Total Cumulative Surface Concentration (μg m^{-3})								
Smoke	3.4		12.2		4.6		21.0	
Dust	12.7		19.0		27.1		64.4	
ABF	4.2		5.8		15.1		26.7	

246
247
248

https://doi.org/10.5194/egusphere-2026-6637
Preprint. Discussion started: 16 November 2026
© Author(s) 2026. CC BY 4.0 License.

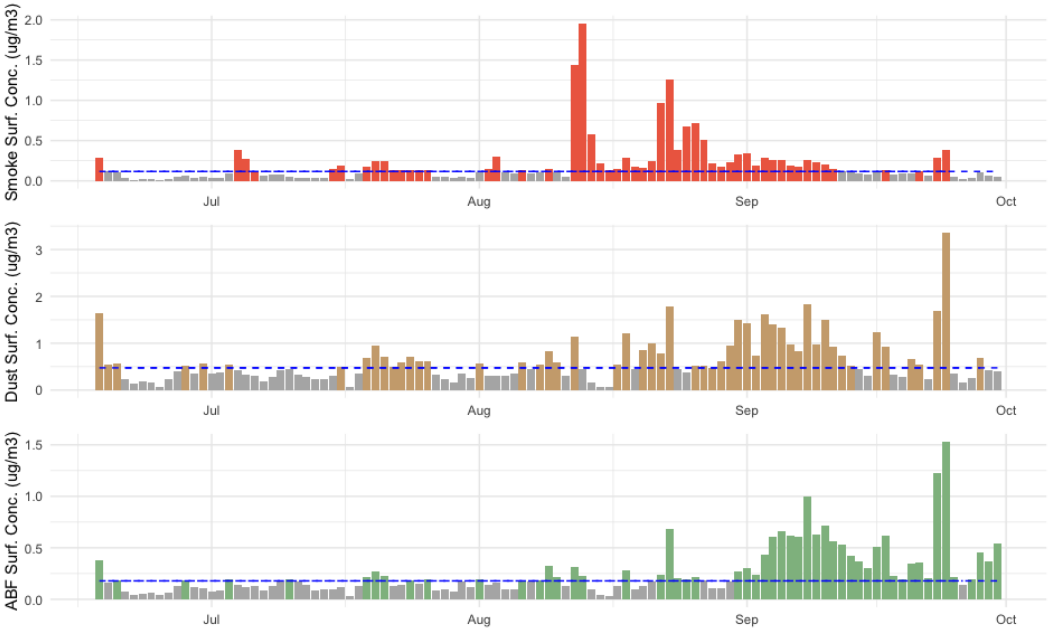


Fig 3. Plots showing high (colored bars) and low (gray bars) surface concentration days for smoke, dust and ABF between June 19 and September 29, 2024. Blue dashed lines indicate median concentrations for each aerosol species. High and low concentration is in reference to above or below the median value. Note the difference in y-axis scales between species.

Table 2: Particle characteristics measured by the SP2-XR during days with high vs. low smoke, dust and ABF surface concentrations. The high and low NAAPS-RA scenarios are in reference to above or below the median NAAPs value for each aerosol species.

	NAAPs Scenario	rBC (cm^{-3})	rBC (ng m^{-3})	Scat. Particle (cm^{-3})	EOD (nm)	EMD (nm)	ECT (nm)
Average ± standard deviations							
Smoke	Low	5.85 ± 1.02	3.74 ± 0.92	64.0 ± 6.0	319 ± 3	199 ± 4	56 ± 1
	High	4.94 ± 0.95	2.69 ± 0.39	38.5 ± 3.3	342 ± 4	184 ± 5	61 ± 1
Dust	Low	6.06 ± 1.29	3.65 ± 0.96	56.7 ± 5.8	324 ± 4	188 ± 3	57 ± 1
	High	4.75 ± 0.56	2.80 ± 0.32	46.2 ± 4.4	338 ± 4	196 ± 6	61 ± 1
ABF	Low	5.16 ± 1.07	3.38 ± 0.95	56.2 ± 5.4	322 ± 4	184 ± 4	58 ± 1
	High	5.63 ± 0.91	3.06 ± 0.35	46.7 ± 4.9	339 ± 5	199 ± 5	60 ± 2
Median and interquartile range (IQR)							
Smoke	Low	3.2 (1.1 - 7.9)	2.1 (0.74 - 4.5)	51.8 (38.3 - 77.3)	313 (304 – 330)	197 (180 – 216)	57 (54 – 58)
	High	3.4 (1.5 - 6.1)	1.9 (0.8 - 3.3)	37.9 (18.1 - 50.6)	343 (318 – 359)	183 (172 – 196)	60 (57 - 63)
Dust	Low	2.8	1.8	47.8	316	188	56

https://doi.org/10.5194/egusphere-2026-6637
Preprint. Discussion started: 16 November 2026
© Author(s) 2026. CC BY 4.0 License.

		(1.2 - 6.3)	(0.8 - 3.6)	(32.7 - 67.3)	(304 – 335)	(175 – 203)	(54 – 60)
	High	4.3 (1.2 - 7.9)	2.8 (0.7 - 3.7)	39.9 (27.2 - 56.7)	339 (317 – 353)	189 (175 – 214)	59 (57 – 62)
ABF	Low	2.8 (0.9 - 6.3)	1.6 (0.6 - 3.3)	47.3 (32.7 - 66.3)	314 (304 – 336)	185 (174– 203)	57 (55 - 61)
	High	4.2 (1.7 - 8.6)	2.6 (1.2 - 4.5)	39.9 (25 – 63.5)	338 (322 – 351)	191 (177 – 212)	58 (56- 61)

Across all three aerosol species, the trend from low to high surface NAAPS-RA aerosol species concentrations is associated higher ECT (Table 2). Comparing SP2-XR particle characteristics across high and low smoke confirms no statistically significant differences in rBC core size, overall diameter, or coating thickness, between high and low smoke events (Figure S1a–j). The only parameter exhibiting a statistically significant difference between high and low smoke scenarios is the total scattering particle concentration (Figure S2a,b)

3.1 Local vs. Long-Range vs. Mixed Transport Days

To explore particle characteristics across source scenarios (local emissions, mostly from fossil fuel combustion from Pituffik Space Base or long-range transport of wildfire derived smoke), the SP2-XR data were classified into three categories as local, long-range or mixed. Briefly, long-range smoke is defined as NAAPS-RA smoke concentration above the median value (0.115 μg m^{-3}) and the wind direction from the West, South, Southwest, or Southeast. Local aerosol contamination is defined as surface smoke concentrations < median value (0.115 μg m^{-3}) and rBC particle concentrations > median (3.18 particles /cm^3). Lastly, "mixed" cases were classified as surface smoke concentration above the median value, but wind direction is from the N, NW or NE (e.g., potential aerosol transport from the Pituffik Space Base power plant). The criteria for each category are further defined in Section 1.5 of the methods.

Across the campaign, 26 days (25%) of the SP2-XR measurements were dominated by local emissions, 36 days (35%) measured long-range transported smoke, and 9 consecutive days (9%) measured "mixed" conditions (Figure 4) where smoke concentrations were above the median (0.115 μg m^{-3}), but the wind was coming from the N, NW, or NE, potentially also bringing local emissions from the base, resupply vessels, or rare, but possible, local shipping. The days with the highest surface smoke concentrations (> 0.5 μg m^{-3}) occurred during long-range transport or "mixed" events, with the maximum long-range smoke events reaching nearly

https://doi.org/10.5194/egusphere-2026-6637
Preprint. Discussion started: 16 November 2026
© Author(s) 2026. CC BY 4.0 License.

2.0 µg m^{-3} on August 13th. Such episodic, high-concentration events are consistent with the trans-Greenland transport of intense Canadian wildfire plumes, which have been shown to drastically alter Arctic background aerosol composition during extreme fire seasons (Adachi et al., 2026; Calì Quaglia et al., 2022).



Fig 4. Bar plot showing daily surface smoke concentration classified by aerosol transport type.

Having isolated local operational plumes from regional transport events, we evaluate the microphysical signatures, specifically core size (EMD), total optical diameter (EOD), and mixing state (ECT), associated with each transport history. Because these microphysical dimensions were completely excluded from the air mass classification criteria, they provide an unbiased assessment of aerosol aging and source characterization. The three emission/transport scenarios also demonstrated significant differences in the median scattering number concentration ($p < 0.001$), with local contamination again containing the highest median scattering number concentration.

To accurately evaluate particle mixing states, a clear physical distinction must be made between the rBC size (EMD; Figure 5a), the total particle optical size (EOD; Figure 5b), and the resulting shell thickness (ECT; Figure 5c). Fresh local emissions were characterized by larger median rBC cores (EMD = 196.3 nm) but smaller total optical particle sizes (EOD = 316.1 nm)

https://doi.org/10.5194/egusphere-2026-6637
Preprint. Discussion started: 16 November 2026
© Author(s) 2026. CC BY 4.0 License.

(Figure 5a, b). Conversely, long-range wildfire smoke exhibited smaller rBC cores (EMD = 184.7 nm), consistent with the preferential scavenging and removal of larger rBC mass cores during long-distance transit, yet larger overall optical particle sizes (EOD = 343.1 nm; $p<0.01$, Figure 5b) likely due to coating by secondary aerosols during transport. This inverse relationship between decreasing core size (EMD) and increasing overall particle size (EOD) explains the marked increase in ECT (median 60.8 nm) observed in aged plumes (median 60.8 nm vs. 56.7 nm local; $p<0.05$; Figure 5c; noting the estimated ±60% uncertainty in derived ECT), demonstrating that non-rBC coating accumulation, rather than core enlargement, drives the total particle volume of long-range Arctic smoke. While these relative differences are statistically significant, we remind the reader that absolute ECT values carry a propagated uncertainty of approximately ±60%.

The long-range transport events contained the highest mean ECT (61.96 nm), which was statistically significantly higher than local scenarios ($p < 0.05$, Figure 5c); however, ECT did not differ significantly between long-range and mixed scenarios. During long-range transport scenarios, particle concentration metrics dropped while the coating thickness increased (Table 3; Figure 5c). During long-range transport, the remaining particles that age during transit can become coated by secondary organic aerosols, such as sulfates that coat rBC particles, resulting in a significantly thicker individual coating (higher ECT; $p<0.05$, Figure 5c). This microphysical evolution is strongly supported by recent individual-particle analyses in Greenland by Adachi et al. (2026), who observed that aged Canadian wildfire plumes are dominated by thick organic matrices embedding soot particles and potassium sulfates. Therefore, the ECT serves as a microphysical signature for differentiating local emissions from aged, long-range smoke.

The average scattering particle concentration was also highest for local aerosol transport events, showing significant reductions in both long-range ($p<0.01$) and mixed scenarios ($p<0.001$, Figure S3). This can be attributed to local airmasses containing higher concentrations of fresh local emissions compared to long-range air masses, which are susceptible to deposition and other removal processes during transit.

Table 3. Average ± standard deviations and Median (IQR) of attributes measured by the SP2-XR during days with aerosol transport classified as local, long-range or mixed. Number of days refers to the total days over the campaign.

https://doi.org/10.5194/egusphere-2026-6637
Preprint. Discussion started: 16 November 2026
© Author(s) 2026. CC BY 4.0 License.

Aerosol Transport Scenario	# Days	rBC (cm^{-3})	rBC (ng m^{-3})	Scat. Particle (cm^{-3})	EOD (nm)	EMD (nm)	ECT (nm)
Average ± Standard Deviation							
Local	26	10.3 ± 1.6	6.9 ± 1.6	64.2 ± 7.0	318.3 ± 3.4	200.6 ± 5.1	55.9 ± 0.8
Long Range	36	5.4 ± 1.3	2.9 ± 0.5	42.4 ± 4.0	343.0 ± 5.3	185.7 ± 6.9	62.0 ± 1.9
Mixed	9	3.4 ± 1.0	2.1 ± 0.6	18.6 ± 3.3	354.8 ± 7.4	167.7 ± 7.7	59.4 ± 0.6
Median and interquartile range (IQR)							
Local	26	8 (5.3 -12.3)	4.5 (3.1 - 6.6)	56.7 (39.8 - 73.1)	316.1 (306.9 – 327.8)	196.3 (185.8 – 210.1)	56.7 (54 – 57.7)
Long Range	36	4.2 (1.4 -5.7)	2.7 (0.9 - 3.3)	39.7 (25.7 - 58.3)	343.1 (321.0 – 357.5)	184.7 (168.9– 196.2)	60.8 (57.2 - 62.8)
Mixed	9	2.4 (1.5 -3.8)	1.6 (0.8 - 2.6)	46.7 (37.8 - 68.3)	357.6 (342.8 –367.9)	177.5 (171.0 – 182.9)	56.4 (54.1 -59.2)

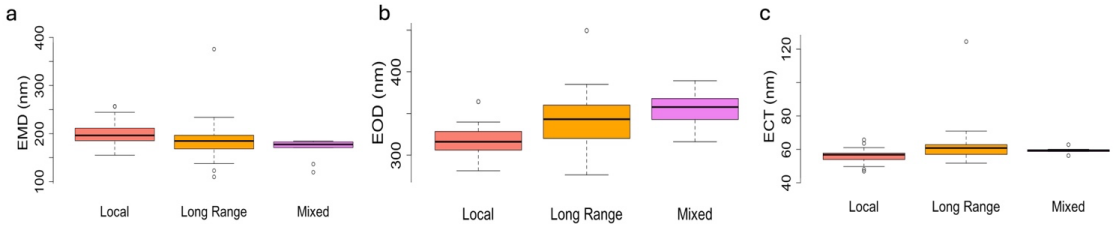


Figure 5. Box plots comparing SP2-XR measured properties across local, long-range, and mixed transport scenarios: a) mass-equivalent core diameter (EMD, nm), b) equivalent optical diameter (EOD, nm), and c) equivalent coating thickness (ECT, nm). Solid horizontal lines indicate median values, box boundaries represent interquartile ranges (IQR), whiskers denote 1.5 × IQR, and open circles indicate individual outliers. Statistical significance among pairwise group comparisons was determined via post-hoc testing (* $p<0.05$, **$p<0.01$, *** $p<0.001$, ns = not significant, $p \geq 0.05$). Across the three variables, no statistically significant differences were observed between Long Range and Mixed scenarios (ns). Significant pairwise differences include: EMD (nm): Local vs. Mixed (*); EOD (nm): Local vs. Long Range (**), Local vs. Mixed (**); ECT (nm): Local vs. Long Range (*).

3.2 Case Studies and NAAPS Smoke AOD Maps

To look deeper into the SP2-XR data within the aerosol transport mechanisms, three case studies were investigated based on the NAAPS smoke surface concentrations. The three scenarios include a local contamination event between September 25-27, a high smoke, long-

https://doi.org/10.5194/egusphere-2026-6637
Preprint. Discussion started: 16 November 2026
© Author(s) 2026. CC BY 4.0 License.

range transport event that occurred between August 12 -18, and a suspected, mixed aerosol transport between August 22-27 (Figure 6; Table S3).

Local Emission Case Study: High rBC mean number concentrations were measured on the SP2-XR (21 cm^{-3}); however, NAAPS data suggest that between September 25 and 27, there were very low mass concentrations of smoke (0.1 μg m^{-3}) and ABF (0.55 μg m^{-3}). This is further confirmed by NAAPS smoke AOD maps (Figure 6a) that show no smoke transport over Greenland during this time. This combined evidence indicates that local contamination from the Pituffik Space Base was likely the source of these rBC particles.

Long-range Transport case study: NAAPS data reveal a high smoke event that occurred between August 12 and 18, which is further illustrated by NAAPS smoke AOD geospatial maps (Figure 6b) that indicate that the smoke was transported from Eastern Canada to the SP2-XR location. During this time, according to the NAAPS, 4.76 μg m^{-3} of smoke was traveled over the surface during the seven days, along with 1.12 μg m^{-3} of ABF. The rBC mean number concentrations measured on the SP2-XR (9 cm^{-3}) were lower than the local emission case study described above, further suggesting long-range transport, whereas the ECT (61 nm) was higher than the local contamination event (48 nm), complementing our findings across the three aerosol scenarios described above.

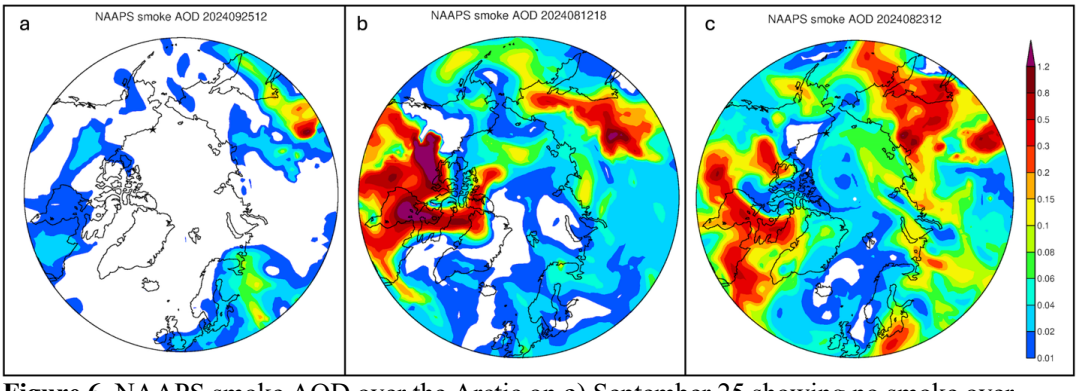


Figure 6. NAAPS smoke AOD over the Arctic on **a**) September 25 showing no smoke over Greenland. **b**) the last day of a high concentration smoke event that occurred between August 12 and 18 showing transport of smoke from Canada to Pituffik, Greenland, and **c**) August 23, the second day of a suspected mixed aerosol transport event that spanned August 22 to 27.

An event with suspected mixed aerosol transport occurred between August 22 and 27, depositing 4.49 μg m^{-3} of smoke and 1.7 μg m^{-3} of ABF over six days. NAAPS smoke AOD

https://doi.org/10.5194/egusphere-2026-6637
Preprint. Discussion started: 16 November 2026
© Author(s) 2026. CC BY 4.0 License.

maps during this event show some smoke transport originating from Canada, with other areas of high smoke AOD over Southern Greenland (Figure 6c). During this time, the mean rBC number concentration (3 cm^{-3}) was lower than both the local and long-range events; however, the median ECT was nearly as high as the long-range event (59 nm). As was pointed out at the beginning of the discussion, this apparent contradiction of lower number concentration yet higher ECT highlights the complexity of the physics of environmental aerosols and their evolution with time and distance. In this case, the results are not necessarily contradictive because the rBC that is produced by the lower temperature combustion from wildfires will interact with other aerosol particles, as well as interstitial gases. Over the many days that the rBC is transported to the measurement site there will be sufficient time for the ECT to increase as these particles grow by coagulation and condensation.

4. Conclusion

As the Arctic undergoes rapid environmental change, accurately predicting the accelerated melting of the GrIS requires an in-depth understanding of aerosol deposition. This study demonstrates that high-resolution, ground-based microphysical measurements can successfully contribute to the untangling of the complex mixture of local and long-range rBC reaching the high Arctic. These findings, consistent with previous airborne and regional Arctic studies (e.g., (Kodros et al., 2018; Kondo et al., 2011), demonstrate an inverse relationship between core size and optical size. This offers direct ground-level in-situ validation that secondary non-rBC coating accumulation drives the total optical volume of aged Arctic smoke.

Measurements from the SP2-XR at THAAO during the summer of 2024 reveal contrasts in the microphysical properties of aerosol particles with different origins and histories. Long-range transport events, such as North American wildfire smoke, exhibit significantly higher ECT (bearing in mind the estimated ±60% uncertainty in absolute ECT values). This higher percentage of non-rBC material on aged particles can alter their hygroscopicity and deposition velocity, meaning that they interact with the Arctic climate system differently than fresh local emissions. Furthermore, once the aerosols are deposited on the surface of the ice sheet, they play a complex role in the ice-albedo feedback. Determination of the parent rBC-source (e.g., local emissions or long-range smoke transport), as determined through SP2-XR measurements described here, can assist with more accurate parametrizations of rBC-deposition in radiative

https://doi.org/10.5194/egusphere-2026-6637
Preprint. Discussion started: 16 November 2026
© Author(s) 2026. CC BY 4.0 License.

transfer models, such as the Snow, Ice, Aerosol, Radiation (SNICAR-ADv4) model (Whicker et al., 2022).

As sea ice retreats and the Arctic becomes increasingly accessible to shipping, tourism, and industrial development, these local emissions will likely capture a larger share of the Arctic aerosol budget, in addition to increasing transport and deposition of smoke from high latitude-wildfires. To accurately model future climate scenarios and albedo reduction on the GrIS, chemical transport models must move beyond bulk mass estimates and account for these specific microphysical differences, namely, the size and coating variations between fresh local contamination and aged, long-range smoke.

Data Availability

The data are available on Zenodo here: https://doi.org/10.5281/zenodo.21479230.

Author Contribution: ALK conceived of the study, acquired funding, and installed/deinstalled the SP2-XR. DB processed the raw SP2-XR data, including sub-setting for local wind parameters. PX extracted the NAAPS-RA surface concentration data. EH conducted data analysis of SP2-XR and NAAPS-RA data and figure generation. FQ assisted with intake-line logistics in the field. GM assisted with pre-installation logistics and THAAO hospitality.

Acknowledgements

The authors thank the NASA ARCSIX Campaign, especially program managers Dr. Hal Maring and Edward Nowottnick and deputy project manager Stevie Phothisane (NASA HQ), as well as ARCSIX Lead-PI Dr. Sebastian Schmidt, for their logistical support with transport to/from the Pituffik Space Base. The authors thank additional THAAO scientists for their support during the field campaign including Alcide Giorgio di Sarra, Monica Tosco, Tatiana di Lorio, and Silvia Becagli. The authors also thank Droplet Measurement Technologies staff members Kristie Stowers, Jesse Steiner, and Dagen Hughes for SP2-XR preparation and logistics, as well as Jacob Dana from CU-Boulder for data analysis and figure contributions.

Competing Interests: The authors declare that they have no conflict of interest.

https://doi.org/10.5194/egusphere-2026-6637
Preprint. Discussion started: 16 November 2026
© Author(s) 2026. CC BY 4.0 License.

Financial Support: This study was supported by the US National Science Foundation Arctic Sciences Award # 2336072, entitled: RAPID: Impacts of Deposition from Smoke-derived Black Carbon on the Greenland Ice Sheet and the Greater Arctic Cryosphere due to Transport from Record Setting Canadian Wildfires. Logistical support was provided by the NASA ARCSIX Field campaign.

References

Adachi, K., Bergner, N., Alden, J., Schmale, J., Ohata, S., and Tobo, Y.: Mixing states and composition of fine aerosol particles in the 2023 Canadian wildfire plumes detected in southern Greenland, EGUsphere, 1–19, https://doi.org/10.5194/egusphere-2026-3518, 2026.

Becagli, S., Caiazzo, L., Di Iorio, T., di Sarra, A., Meloni, D., Muscari, G., Pace, G., Severi, M., and Traversi, R.: New insights on metals in the Arctic aerosol in a climate changing world, Science of The Total Environment, 741, 140511, https://doi.org/10.1016/j.scitotenv.2020.140511, 2020.

Bond, T. C., Doherty, S. J., Fahey, D. W., Forster, P. M., Berntsen, T., DeAngelo, B. J., Flanner, M. G., Ghan, S., Kärcher, B., Koch, D., Kinne, S., Kondo, Y., Quinn, P. K., Sarofim, M. C., Schultz, M. G., Schulz, M., Venkataraman, C., Zhang, H., Zhang, S., Bellouin, N., Guttikunda, S. K., Hopke, P. K., Jacobson, M. Z., Kaiser, J. W., Klimont, Z., Lohmann, U., Schwarz, J. P., Shindell, D., Storelvmo, T., Warren, S. G., and Zender, C. S.: Bounding the role of black carbon in the climate system: A scientific assessment, JGR Atmospheres, 118, 5380–5552, https://doi.org/10.1002/jgrd.50171, 2013.

Buchholz, R. R., Park, M., Worden, H. M., Tang, W., Edwards, D. P., Gaubert, B., Deeter, M. N., Sullivan, T., Ru, M., Chin, M., Levy, R. C., Zheng, B., and Magzamen, S.: New seasonal pattern of pollution emerges from changing North American wildfires, Nat Commun, 13, 2043, https://doi.org/10.1038/s41467-022-29623-8, 2022.

Calì Quaglia, F., Meloni, D., Muscari, G., Di Iorio, T., Ciardini, V., Pace, G., Becagli, S., Di Bernardino, A., Cacciani, M., Hannigan, J. W., Ortega, I., and di Sarra, A. G.: On the Radiative Impact of Biomass-Burning Aerosols in the Arctic: The August 2017 Case Study, Remote Sensing, 14, 313, https://doi.org/10.3390/rs14020313, 2022.

Ciardini, V., Muscari, G., Di Sarra, A., Di Iorio, T., Meloni, D., Pace, G., Scarchilli, C., Calì Quaglia, F., Tosco, M., Bagiacchi, P., Cannataro, G., and Iaccarino, A.: Meteorological data at the precipitation mast at the Thule High Arctic Atmospheric Observatory (THAAO_Met_Prec), https://doi.org/10.13127/THAAO/MET_PREC, 2026., 2026.

Cordero, R. R., Sepúlveda, E., Feron, S., Damiani, A., Fernandoy, F., Neshyba, S., Rowe, P. M., Asencio, V., Carrasco, J., Alfonso, J. A., Llanillo, P., Wachter, P., Seckmeyer, G., Stepanova, M., Carrera, J. M., Jorquera, J., Wang, C., Malhotra, A., Dana, J., Khan, A. L., and Casassa, G.:

https://doi.org/10.5194/egusphere-2026-6637
Preprint. Discussion started: 16 November 2026
© Author(s) 2026. CC BY 4.0 License.



Black carbon footprint of human presence in Antarctica, Nat Commun, 13, 984, https://doi.org/10.1038/s41467-022-28560-w, 2022.

Doherty, S. J., Warren, S. G., Grenfell, T. C., Clarke, A. D., and Brandt, R. E.: Light-absorbing impurities in Arctic snow, Atmos. Chem. Phys., 10, 11647–11680, https://doi.org/10.5194/acp-10-11647-2010, 2010.

Eckhardt, S., Quennehen, B., Olivié, D. J. L., Berntsen, T. K., Cherian, R., Christensen, J. H., Collins, W., Crepinsek, S., Daskalakis, N., Flanner, M., Herber, A., Heyes, C., Hodnebrog, Ø., Huang, L., Kanakidou, M., Klimont, Z., Langner, J., Law, K. S., Lund, M. T., Mahmood, R., Massling, A., Myriokefalitakis, S., Nielsen, I. E., Nøjgaard, J. K., Quaas, J., Quinn, P. K., Raut, J.-C., Rumbold, S. T., Schulz, M., Sharma, S., Skeie, R. B., Skov, H., Uttal, T., von Salzen, K., and Stohl, A.: Current model capabilities for simulating black carbon and sulfate concentrations in the Arctic atmosphere: a multi-model evaluation using a comprehensive measurement data set, Atmospheric Chemistry and Physics, 15, 9413–9433, https://doi.org/10.5194/acp-15-9413-2015, 2015.

Flanner, M. G., Zender, C. S., Randerson, J. T., and Rasch, P. J.: Present-day climate forcing and response from black carbon in snow, Journal of Geophysical Research: Atmospheres, 112, https://doi.org/10.1029/2006JD008003, 2007.

Frossard, A. A., Shaw, P. M., Russell, L. M., Kroll, J. H., Canagaratna, M. R., Worsnop, D. R., Quinn, P. K., and Bates, T. S.: Springtime Arctic haze contributions of submicron organic particles from European and Asian combustion sources, Journal of Geophysical Research: Atmospheres, 116, https://doi.org/10.1029/2010JD015178, 2011.

Heutte, B., Rogers, S., Angot, H., Beck, I., Bergner, N., Creamean, J. M., Dada, L., Henning, S., Jokinen, T., Lonardi, M., Nenes, A., Petäjä, T., Pohorsky, R., Pratt, K. A., Quéléver, L. L. J., and Schmale, J.: The role of local shipping emissions in aerosol-cloud interactions in the central Arctic, Environ. Res. Lett., 21, 104014, https://doi.org/10.1088/1748-9326/ae6673, 2026.

Khan, A. L., Wagner, S., Jaffe, R., Xian, P., Williams, M., Armstrong, R., and McKnight, D.: Dissolved black carbon in the global cryosphere: Concentrations and chemical signatures: DBC in the Global Cryosphere, Geophys. Res. Lett., 44, 6226–6234, https://doi.org/10.1002/2017GL073485, 2017a.

Khan, A. L., Dierssen, H., Schwarz, J. P., Schmitt, C., Chlus, A., Hermanson, M., Painter, T. H., and McKnight, D. M.: Impacts of coal dust from an active mine on the spectral reflectance of Arctic surface snow in Svalbard, Norway, J. Geophys. Res. Atmos., 122, 1767–1778, https://doi.org/10.1002/2016JD025757, 2017b.

Khan, A. L., Xian, P., and Schwarz, J. P.: Black carbon concentrations and modeled smoke deposition fluxes to the bare-ice dark zone of the Greenland Ice Sheet, The Cryosphere, 17, 2909–2918, https://doi.org/10.5194/tc-17-2909-2023, 2023.

Kodros, J. K., Hanna, S. J., Bertram, A. K., Leaitch, W. R., Schulz, H., Herber, A. B., Zanatta, M., Burkart, J., Willis, M. D., Abbatt, J. P. D., and Pierce, J. R.: Size-resolved mixing state of black carbon in the Canadian high Arctic and implications for simulated direct radiative effect,

https://doi.org/10.5194/egusphere-2026-6637
Preprint. Discussion started: 16 November 2026
© Author(s) 2026. CC BY 4.0 License.

Atmospheric Chemistry and Physics, 18, 11345–11361, https://doi.org/10.5194/acp-18-11345-2018, 2018.

Kondo, Y., Matsui, H., Moteki, N., Sahu, L., Takegawa, N., Kajino, M., Zhao, Y., Cubison, M. J., Jimenez, J. L., Vay, S., Diskin, G. S., Anderson, B., Wisthaler, A., Mikoviny, T., Fuelberg, H. E., Blake, D. R., Huey, G., Weinheimer, A. J., Knapp, D. J., and Brune, W. H.: Emissions of black carbon, organic, and inorganic aerosols from biomass burning in North America and Asia in 2008, Journal of Geophysical Research: Atmospheres, 116, https://doi.org/10.1029/2010JD015152, 2011.

Law, K. S. and Stohl, A.: Arctic air pollution: origins and impacts, Science, 315, 1537–1540, https://doi.org/10.1126/science.1137695, 2007.

Lynch, P., Reid, J. S., Westphal, D. L., Zhang, J., Hogan, T. F., Hyer, E. J., Curtis, C. A., Hegg, D. A., Shi, Y., Campbell, J. R., Rubin, J. I., Sessions, W. R., Turk, F. J., and Walker, A. L.: An 11-year global gridded aerosol optical thickness reanalysis (v1.0) for atmospheric and climate sciences, Geosci. Model Dev., 9, 1489–1522, https://doi.org/10.5194/gmd-9-1489-2016, 2016.

Markowicz, K. M., Pakszys, P., Ritter, C., Zielinski, T., Udisti, R., Cappelletti, D., Mazzola, M., Shiobara, M., Xian, P., Zawadzka, O., Lisok, J., Petelski, T., Makuch, P., and Karasiński, G.: Impact of North American intense fires on aerosol optical properties measured over the European Arctic in July 2015, Journal of Geophysical Research: Atmospheres, 121, 14,487-14,512, https://doi.org/10.1002/2016JD025310, 2016.

Ranjbar, K., O'Neill, N. T., Lutsch, E., McCullough, E. M., AboEl-Fetouh, Y., Xian, P., Strong, K., Fioletov, V. E., Lesins, G., and Abboud, I.: Extreme smoke event over the high Arctic, Atmospheric Environment, 218, 117002, https://doi.org/10.1016/j.atmosenv.2019.117002, 2019.

Reid, J. S., Hyer, E. J., Prins, E. M., Westphal, D. L., Zhang, J., Wang, J., Christopher, S. A., Curtis, C. A., Schmidt, C. C., Eleuterio, D. P., Richardson, K. A., and Hoffman, J. P.: Global Monitoring and Forecasting of Biomass-Burning Smoke: Description of and Lessons From the Fire Locating and Modeling of Burning Emissions (FLAMBE) Program, IEEE Journal of Selected Topics in Applied Earth Observations and Remote Sensing, 2, 144–162, https://doi.org/10.1109/JSTARS.2009.2027443, 2009.

Schmale, J., Zieger, P., and Ekman, A. M. L.: Aerosols in current and future Arctic climate, Nat. Clim. Chang., 11, 95–105, https://doi.org/10.1038/s41558-020-00969-5, 2021.

Schmale, J., Sharma, S., Decesari, S., Pernov, J., Massling, A., Hansson, H.-C., von Salzen, K., Skov, H., Andrews, E., Quinn, P. K., Upchurch, L. M., Eleftheriadis, K., Traversi, R., Gilardoni, S., Mazzola, M., Laing, J., and Hopke, P.: Pan-Arctic seasonal cycles and long-term trends of aerosol properties from 10 observatories, Atmospheric Chemistry and Physics, 22, 3067–3096, https://doi.org/10.5194/acp-22-3067-2022, 2022.

Schwarz, J. P., Gao, R. S., Fahey, D. W., Thomson, D. S., Watts, L. A., Wilson, J. C., Reeves, J. M., Darbeheshti, M., Baumgardner, D. G., Kok, G. L., Chung, S. H., Schulz, M., Hendricks, J., Lauer, A., Kärcher, B., Slowik, J. G., Rosenlof, K. H., Thompson, T. L., Langford, A. O., Loewenstein, M., and Aikin, K. C.: Single-particle measurements of midlatitude black carbon

https://doi.org/10.5194/egusphere-2026-6637
Preprint. Discussion started: 16 November 2026
© Author(s) 2026. CC BY 4.0 License.

and light-scattering aerosols from the boundary layer to the lower stratosphere, Journal of Geophysical Research: Atmospheres, 111, https://doi.org/10.1029/2006JD007076, 2006.

Schwarz, J. P., Spackman, J. R., Fahey, D. W., Gao, R. S., Lohmann, U., Stier, P., Watts, L. A., Thomson, D. S., Lack, D. A., Pfister, L., Mahoney, M. J., Baumgardner, D., Wilson, J. C., and Reeves, J. M.: Coatings and their enhancement of black carbon light absorption in the tropical atmosphere, Journal of Geophysical Research: Atmospheres, 113, https://doi.org/10.1029/2007JD009042, 2008a.

Schwarz, J. P., Gao, R. S., Spackman, J. R., Watts, L. A., Thomson, D. S., Fahey, D. W., Ryerson, T. B., Peischl, J., Holloway, J. S., Trainer, M., Frost, G. J., Baynard, T., Lack, D. A., de Gouw, J. A., Warneke, C., and Del Negro, L. A.: Measurement of the mixing state, mass, and optical size of individual black carbon particles in urban and biomass burning emissions, Geophysical Research Letters, 35, https://doi.org/10.1029/2008GL033968, 2008b.

Stephens, M., Turner, N., and Sandberg, J.: Particle identification by laser-induced incandescence in a solid-state laser cavity, Appl Opt, 42, 3726–3736, https://doi.org/10.1364/ao.42.003726, 2003.

Stohl, A., Klimont, Z., Eckhardt, S., Kupiainen, K., Shevchenko, V. P., Kopeikin, V. M., and Novigatsky, A. N.: Black carbon in the Arctic: the underestimated role of gas flaring and residential combustion emissions, Atmospheric Chemistry and Physics, 13, 8833–8855, https://doi.org/10.5194/acp-13-8833-2013, 2013.

Taylor, P. C., Sorooshian, A., Ueyama, R., Schmidt, S., Abboud, I., Allison, Q., Barry, K., Becker, S., Bender, H. A., Bennett, J. R., Blair, J. B., Bohn, N., Boisvert, L., Brown, M. D., Bruintjes, R., Bucholtz, A., Buzanowicz, M., Cairns, B., Calì Quaglia, F., Chemyakin, E., Chen, B., Chen, G., Chen, H., Chen, Y.-W., Cheng, Z., China, S., Chirica, D., Choi, Y., Colarco, P., Collister, B., Crosbie, E., Cross, M. J., Daniels, J., DeMott, P., DiGangi, J. P., Di Sarra, A. G., Diskin, G. S., Dolinar, E. K., Edwards, E.-L., Ephraim, S., Evangeliou, N., Foskinis, R., Gallo, F., Gao, L., Gómez-Amo, J. L., Gonzalez, D., Groot Zwaaftink, C., Gupta, P., Heckman, I., Hendrickson, M., Hilario, M. R. A., Hirata, K., Hofton, M., Holen, A. L., Im, U., Khan, A. L., Kahn, R., Korolev, A. V., Kreidenweis, S., Krumpen, T., Kurtz, N., Lait, L., Lamkin, B., Landy, J., Lata, N. N., Lawson, P., LeBlanc, S., Leavor, S., Li, J., Markus, T., Maring, H., Massling, A. H., Mavis, C., McGinnity, F., Meyer, K., Mojica, G., Moore, R. H., Morris, P., Muscari, G., Nataraja, V., Nehrir, A. R., Nenes, A., Nowottnick, E. P., Ottaviani, M., Parker, C., Patnaude, R., Perez, M., Perkins, R. J., Peterson, C., Petty, A., Phothisane, S., Polashenski, C., Pratt, K. A., Preisler, K. M., Prytherch, J., Rabine, D., Redemann, J., Ryoo, J.-M., Schlosser, J. S., Selimovic, V., Shook, M. A., Silverman, M., Skov, H., Smirnov, A., Soloff, C., Solomon, A., Stamnes, S., Takeishi, A., Thompson, D. R., Thornhill, K. L., Tilling, R., Tjernström, M., Tosco, M., Valdelomar, P. C., Van Gilst, D., Wang, J., Wang, Z., Wasilewski, A., Wendisch, M., Wilder, B., Winstead, E. L., Wu, A., Xian, P., Zamora, L. M., Zhang, J., Zhang, L., Zhang, L., Ziemba, L., and Zuidema, P.: The Arctic Radiation-Cloud-Aerosol-Surface Interaction Experiment (ARCSIX) airborne campaign dataset, https://doi.org/10.5194/essd-2026-241, 24 July 2026., 2026.

https://doi.org/10.5194/egusphere-2026-6637
Preprint. Discussion started: 16 November 2026
© Author(s) 2026. CC BY 4.0 License.



592 Wang, Q., Jacob, D. J., Fisher, J. A., Mao, J., Leibensperger, E. M., Carouge, C. C., Le Sager, P.,
593 Kondo, Y., Jimenez, J. L., Cubison, M. J., and Doherty, S. J.: Sources of carbonaceous aerosols
594 and deposited black carbon in the Arctic in winter-spring: implications for radiative forcing,
595 Atmos. Chem. Phys., 11, 12453–12473, https://doi.org/10.5194/acp-11-12453-2011, 2011.

596 Whicker, C. A., Flanner, M. G., Dang, C., Zender, C. S., Cook, J. M., and Gardner, A. S.:
597 SNICAR-ADv4: a physically based radiative transfer model to represent the spectral albedo of
598 glacier ice, The Cryosphere, 16, 1197–1220, https://doi.org/10.5194/tc-16-1197-2022, 2022.

599 Winiger, P., Andersson, A., Eckhardt, S., Stohl, A., Semiletov, I. P., Dudarev, O. V., Charkin,
600 A., Shakhova, N., Klimont, Z., Heyes, C., and Gustafsson, Ö.: Siberian Arctic black carbon
601 sources constrained by model and observation, Proceedings of the National Academy of
602 Sciences, 114, E1054–E1061, https://doi.org/10.1073/pnas.1613401114, 2017.

603 Xian, P., Zhang, J., O'Neill, N. T., Toth, T. D., Sorenson, B., Colarco, P. R., Kipling, Z., Hyer,
604 E. J., Campbell, J. R., Reid, J. S., and Ranjbar, K.: Arctic spring and summertime aerosol optical
605 depth baseline from long-term observations and model reanalyses – Part 1: Climatology and
606 trend, Atmospheric Chemistry and Physics, 22, 9915–9947, https://doi.org/10.5194/acp-22-9915-
607 2022, 2022a.

608 Xian, P., Zhang, J., O'Neill, N. T., Reid, J. S., Toth, T. D., Sorenson, B., Hyer, E. J., Campbell,
609 J. R., and Ranjbar, K.: Arctic spring and summertime aerosol optical depth baseline from long-
610 term observations and model reanalyses – Part 2: Statistics of extreme AOD events, and
611 implications for the impact of regional biomass burning processes, Atmos. Chem. Phys., 22,
612 9949–9967, https://doi.org/10.5194/acp-22-9949-2022, 2022b.

613 Zanatta, M., Laj, P., Gysel, M., Baltensperger, U., Vratolis, S., Eleftheriadis, K., Kondo, Y.,
614 Dubuisson, P., Winiarek, V., Kazadzis, S., Tunved, P., and Jacobi, H.-W.: Effects of mixing state
615 on optical and radiative properties of black carbon in the European Arctic, Atmospheric
616 Chemistry and Physics, 18, 14037–14057, https://doi.org/10.5194/acp-18-14037-2018, 2018.

617 Zhao, P., Li, Y., Zhang, C., Kang, T., He, Z., Huang, G., Zhang, S., Zhang, X., Xu, Y., and
618 Kong, W.: Arctic Sea Route access reshapes global shipping carbon emissions, Nat Commun,
619 16, 8431, https://doi.org/10.1038/s41467-025-64437-4, 2025.

620

621 Thule High Arctic Atmospheric Observatory. (n.d.). *Thule Atmos Italy – Home Page*. Retrieved
622 January 27, 2026, from www.thuleatmos-it.it

623
624
625